BACHELOR THESIS

THESIS SUBMITTED FOR THE DEGREE OF BACHELOR OF SCIENCE

Modeling Rapid Melt Growth for III-V integration on Si

Author:
Zahra BANEEN

Supervisors:
Mattias BORG
Jonas JOHANSSON

PROJECT DURATION: JAN TO MAY 2017

LUND UNIVERSITY

Abstract

High quality III-V semiconductors on silicon substrate can make for significant progress in gate electrostatics and optoelectronic devices. Indium antimonide with its inviting properties can play a key role to further facilitate devise integration. But the question is, is it possible to obtain high quality III-V semiconductors on low cost silicon and still be able to manufacture it at large scale? The answer is yes! With the technique "Rapid Melt Growth" defect free lattice mismatch materials can be produced on large scale. The resulting material is free of crystallographic defects and is high in purity. To be able to use rapid melt growth to produce high quality single crystalline material, the thermodynamic parameters for nucleation and growth velocity needs to be known. The problem arises when these parameters cannot readily be found in literature and require long term experiments. In this thesis, the thermodynamic parameters are found from relevant equations and assumptions based on literature. Using these parameters, a temperature window of 108 K was found, which is large enough and hence leads to long epitaxial length before random nucleation dominates. This length was found to be 2.61 mm, which is good enough for most device fabrication. The results can be applied for materials having similar properties to Indium antimonide. Nonetheless changing some of the parameters further improved the results for nucleation and growth i.e. in the future those parameters need to be reconsidered.

Acknowledgments

This bachelor project has been an amazing experience and I take this opportunity to appreciate the help and the support of the many people whose contribution to the presented thesis is of vital importance. Firstly, I would like to sincerely thank my main supervisor, Mattias Borg. Thank you so much for giving me the opportunity to take this project. I have always been wanting to work in this specialized field. Thank you very much for your guidance and encouragement throughout the project. Thank you for all the great literatures that you provided and all the help that made me finish my thesis on time. Thank you for all the feedbacks.

I would like to thank my co-supervisor, Jonas Johansson. Thank you so much for your support through out the project. You were always there to help me out, give advice and give detail explanations of the theory. Thanks for always keeping a check on my project time plan and thanks for the feedbacks.

I wish to express my sincere thanks to the Faculty of Physics and Engineering, for providing me with all the necessary facilities for this project. In addition a thank you to Professor Erik Lind who helped me find my Supervisor based on my interest area and a thank you to the coordinator of education at the Nano Lund, Dan Hessman who helped me find my co-supervisor on time. Thanks to the research committee at the Nano Lund for interesting seminar and discussion on nano wires. It really expand my understanding in nano science and was a good way to know about the ongoing research on the faculty and the rest of the world.

At last I would like to express my deepest respect and gratitude to my parents without whom I would not have been able to reach this far. Thank you very much for you constant support, encouragement and everything. Special thanks to my sister and her family, you people have always been there for me. Thanks to my friends for their quality time. I am truly grateful for their guidance and encouragement, thanks for all the happy memories. Life is much fun with you all.

Contents

1 Theory **3**
- 1.1 First order phase transitions . . . 3
- 1.2 Nucleation . . . 4
  - 1.2.1 Homogeneous nucleation . . . 6
  - 1.2.2 Heterogeneous nucleation . . . 7
- 1.3 Growth velocity . . . 9

2 Method **10**
- 2.1 Rapid melt growth . . . 10
- 2.2 Parameter Analysis . . . 11

3 Results and Discussion **14**
- 3.1 Results . . . 14
- 3.2 Further analysis . . . 17
- 3.3 Discussion . . . 18

4 Conclusion and Outlook **20**

Introduction

In today's semiconductor technology, devices are mostly built in the micrometer scale that plays vital role in device integration. High quality III-V semiconductor micro structures on silicon/oxide substrate can facilitate device integration for future generation of electronic devises. Therefore, it is important to study the techniques that can develop high quality III-V semiconductors on silicon. Even though there exist many techniques to achieve high quality III-V semiconductors, unfortunately most of them cannot be applied for the manufacturing of large scale products. For example, the use of the technique "direct epitaxial growth" necessitates a thick buffer layer to reduce lattice mismatch. This makes integration more complex and unwelcome. On the other hand, "Local epitaxial growth" in small seed holes can reduce crystal defects due to lattice mismatch but nevertheless this technique is so far not applied on large scale [1]. On the contrary, the technique" Rapid melt growth" is able to achieve large scale structures and gives very high quality III-V semiconductor micro structures on Si substrate. By applying rapid melt growth or RMG technique, the resulting structure is significantly less harmed, is free of crystallographic defects, and is very high in purity. More essentially carrier lifetime is not greatly affected [2]. These results are very promising and is a major step towards the rational growth of III-V micrometer structures for device applications [2].

Silicon has been the primary semiconductor to drive the microelectronics industry. But as the scaling of silicon devices have become more difficult, researchers are now looking for different channel material to upgrade the capacity of silicon [3], indium antimonide has attracted much attention due to its distinctive properties. Its properties and applications are discussed in the following paragraph.

Indium antimonide or InSb is a semiconductor compound made from the elements indium and antimony and it belongs to the III-V group. The crystal structure of InSb is zincblende. Each indium(In) atom is attached to four antimony(Sb) atom. Antimony has five valence electrons, three of which makes a covalent bond to indium and two of them are free for interaction and can create electron pair in a bulk of semiconductor [4].
InSb has the highest lattice constant of 6.48 Å at 298 K and highest electron mobility of 7.7×10^4 $cm^2\ V^{-1}s^{-1}$ at 300 K amongst all semiconductors. It also has the lowest melting temperature of 805 K. It has a narrow direct band gap of 0.17 eV at 300 K which is the smallest of all III-V semiconductors [5].
InSb have been used in galvanomagnetic Seeback devices due to its high electron mobility [6] and low thermal conductivity. It is also used in many detectors, at room temperature these sensors can detect NO_2 at a scale of 1 ppm, which is five times smaller than the allowed limit. InSb nanowires are used in field effect transistors due to very high current saturation and effective transconductance [7]. It has high spin-orbit interaction and can be used in quantum Majorana devices [8]. InSb nanowires can be used to fabricate atomic scale devices, such devices were

used to discover Majorana particles.

Integrating indium antimonide on low cost Si substrates by rapid melt growth has further potential to make substantial progress e.g. in gate electrostatics. RMG takes into account nucleation and growth rate. To use the RMG method to produce high quality crystals of InSb, the epitaxial growth seeded by silicon should travel a long enough distance before the reaction is obstructed by the unseeded nucleation. Otherwise the arbitrary unseeded nucleation will give rise to polycrystalline InSb instead of single crystalline film. During the solidification process both the growth velocity and the nucleation rate will vary with the temperature. Initially they increase with undercooling because of the increase in the driving force for the crystallization, then it reaches the maximum value and then decrease as the temperature drops because the motion of atoms slows down. Normally the temperature for maximum growth velocity is higher than the temperature for maximum nucleation rate. As a result, when the liquid InSb is cooled down, it is expected that there exists a temperature window below but close to the melting temperature where epitaxial growth is maximum and unseeded nucleation is negligible [9]. Depending on temperature gradient and cooling rate, the crystallization rate will vary, which can strongly impact the crystal quality and homogeneity. It is therefore important to obtain a model for the rate of crystallization as a function of temperature. Furthermore, with the same thermodynamic parameters the model can be extended to find the maximum length of the single crystal before the arbitrary nucleation becomes dominant. As such it requires to establish a relation for the cooling rate as a function of the maximum length of the crystal.

This project aims to create a theoretical model for nucleation and crystal growth of InSb by rapid melt growth. The concept is based on to find the temperature window where growth rate is maximum over nucleation and to find the maximum length of a single crystal before nucleation becomes unavoidable. To achieve this, the thermodynamic parameters for InSb needs to be known, the problem arises because these parameters are not readily available in literature. The project specifically aims to find these parameters as reformable as possible in order to achieve high quality InSb to possibly help device integration.

Chapter 1

Theory

Most materials undergo phase transition e.g. from liquid to solid state. Solidification of a pure undercooled melt is an example of a first order phase transition. The thermodynamic force given by the under-cooling must achieve two processes namely nucleation and growth. Before going into the details of nucleation and growth we first look at phase transitions.

1.1 First order phase transitions

Thermodynamic equilibrium requires the free energy to be minimized. For a process that occurs at constant pressure P, we minimize the Gibbs free energy $G = H - TS$, where H and S are the enthalpy and entropy respectively and T is the temperature. A first order phase transition has two distinctive phases that are mostly symmetrical around a sharp interface. Each phase is defined by free energy as a function of temperature. The free energy of the two phases intersects at melting temperature, T_m , also called a transition point. A liquid that is cooled infinitely slowly will solidify at the melting temperature. Nonetheless the real phase transitions takes place at finite rates and hence involves a path away from equilibrium that gives the driving force for the transformation. The system at equilibrium i.e. $T_l < T_m$, where T_l is the nucleation temperature, will arrange itself in a phase with lowest free energy [9].
The free energy of solid-liquid phase transition as a function of temperature is shown in fig. 1.1. The two phases intersect at T_m. At equilibrium, the free energy curve for the liquid phase is above the T_m and for the solid phase it is below T_m. The liquid has free energy greater than solid by a factor of ΔG_V. As solidification reduces the free energy of the system, ΔG_V provides the driving force for the phase transition.
The following expression holds for ΔG_V :

$$\Delta G_V = \Delta H_F - \Delta T_m \frac{\Delta H_F}{T_m} = \Delta H_F \left(\frac{T_m - T_l}{T_m} \right) \quad (1.1)$$

The undercooling i.e. $T_m - T_l$ gives the driving force for the nucleation and growth. This expression hold for most of the solidification process since $T_l < T_m$ excluding the case for very rapid cooling where the system can be highly undercooled.

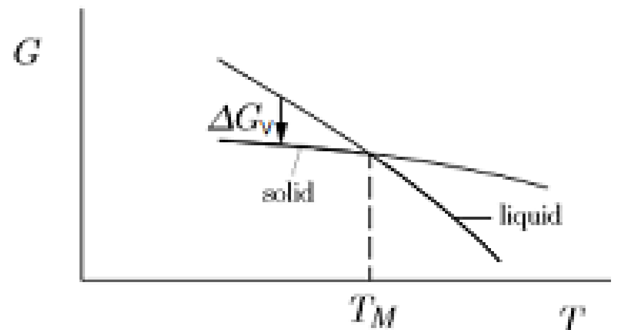

Figure 1.1: *free energy versus temperature [10]*

1.2 Nucleation

Nucleation can be seen as the first step for the development of a new phase transition or a new structure through self-assembly. Nucleation is impurity sensitive therefore it is important to differentiate two types of nucleation namely homogeneous nucleation and heterogeneous nucleation. Homogeneous nucleation takes place away from the surface and heterogeneous occurs at the surface of the system. Fig. 1.2 below simply illustrates the two types of nucleation.

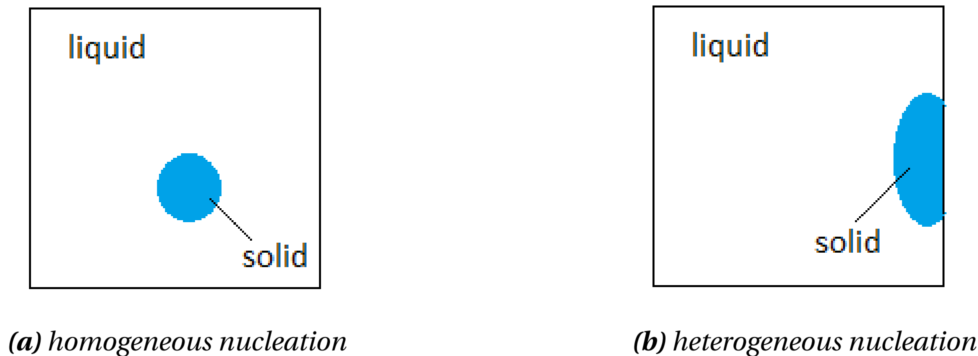

(a) homogeneous nucleation *(b) heterogeneous nucleation*

Figure 1.2: *Nucleation*

Classical nucleation theory gives the free energy barrier by taking the phase droplet of the phase as consisting of a bulk core enclosed by an interface [11]. Classical nucleation theory has been applied by Liu [12] and Feng [13] on RMG to learn about the magnitude of the process window, this was achieved by making comparison between the growth rate with the homogeneous and heterogeneous nucleation rates. Since the RMG process is initiated under equilibrium condition, classical theory seems to give reliable results. It is assumed that during phase change there is no change in volume, even though for InSb a density increase of approximately 5% [14]is observed during melting, but this is assumed to be negligible. Another assumption is that atomic motion is dominant for growth velocity, meaning the rate of latent heat flow is very large at the interface and that growth velocity of crystal in unaffected by small heat losses.

Nucleation barrier

The free energy change corresponding to the formation of a solid particle from an undercooled liquid depends on two "competitive" terms, depicted in fig. 1.3 below. The negative volume term; which is related to massive condensation energy and the positive surface term which is related to the formation of the new interface area between solid-liquid.
The formation of a solid nucleus gives rise to the Gibbs free energy change:

$$\Delta G = \underbrace{\frac{-V}{V_A}\Delta g_A}_{\text{negative below } T_m} + \underbrace{A\gamma_{SL}}_{\text{always positive}} \tag{1.2}$$

V is the volume of sphere
V_A is the volume assumed to contain single atom
A is the interface area
γ_{SL} is the solid-liquid interface energy
Δg_A is the free energy change per atom

If in a solid particle, N is the number of atoms, the following applies:

$$\Delta G = -N\Delta g_A + nN^{2/3}\gamma_{SL} \tag{1.3}$$

n is the shape factor and for spherical solid particles with a radius r we have:

$$N = \frac{4}{3V_A}\pi r^3 \tag{1.4}$$

Since the volume term is negative and the surface term is positive the sum of the two will result in a peak. The peak occurs when the number of atoms is equal to the critical number of atoms, or $N = N^*$ as shown in fig. 1.3.

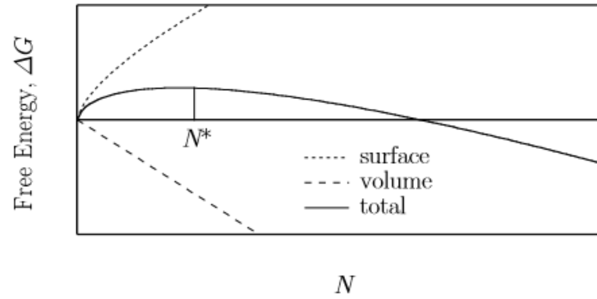

Figure 1.3: *Shows free energy versus number of atoms. The sum of the surface and volume term gives rise to peak at $N = N^*$ [9]*

The addition of a solid particle will influence the free energy. If $N < N^*$, adding an atom will increase the free energy as a result the solid particle will diminish. If $N > N^*$, then adding an atom will decrease the free energy and as a result the solid particle will grow. Adding and atom when $N = N^*$ is the nucleation process. This gives a nuclei that will decrease its free energy by growing.
The free energy change, ΔG , for the spherical particle at the critical radius, r^*,: critical radius is the least size that a particle should attain for the new phase to be stable and grow, is given by:

$$\Delta G^* = \frac{-4}{3}\pi(r^*)^3\Delta G_V + 4\pi(r^*)^2\gamma_{SL} \tag{1.5}$$

where γ_{SL} is the solid liquid interface energy, given:

$$r^* = \frac{2\gamma_{SL}}{\Delta G_V} \tag{1.6}$$

Substituting r^* into eq. 1.5 gives the nucleation barrier as :

$$\Delta G^* = \frac{16\pi\gamma_{SL}^3}{3\Delta G_V^2} = \frac{16\pi V_A^2 T_m^2 \gamma_{SL}^3}{3\Delta h_f^2(\Delta T)^2} \tag{1.7}$$

Fig. 1.4 shows how the free energy varies with the radius.

From the figure, it is clear that as the particle size grows to r_0, the nucleation barrier drops to zero. The nucleation barrier thereafter continues to decreases below zero as it is thermodynamically favored. The nucleation in this figure can be divided into three thermodynamic regimes and the argument is more or less similar to that for fig. 1.3. Firstly, as r increases, ΔG increases primary due to the increase in surface energy, meaning that the growth of particle or nucleation in this area is not thermodynamically favored and most particles will return to the liquid phase. This is common for homogeneous nucleation. Secondly, as the particle size reaches r^* and passes $\Delta G(r^*)$, any increase in particle size will decrease the free energy-a trend favored for solidification. At last when particles pass beyond r_0, the nucleation barrier will become more negative and at this point the growth of a particle is largely favored and this will result in the formation of bulk-phase solid.

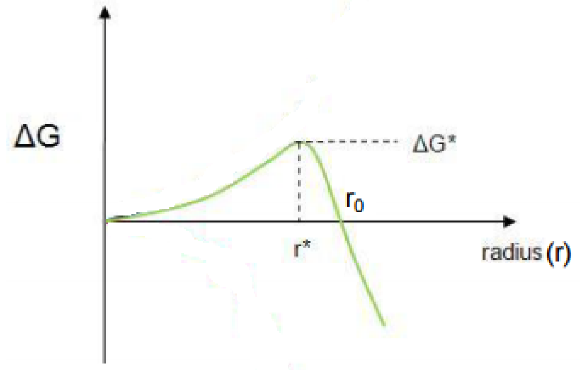

Figure 1.4: *free energy versus the radius [15]*

1.2.1 Homogeneous nucleation

Homogeneous nucleation takes place at very large undercoolings compared to the heterogeneous nucleation. It is important to observe homogeneous nucleation, since the onset of homogeneous nucleation gives the highest limit of undercooling that exist for a melt. In presence of heterogeneous nucleation, homogeneous nucleation is highly unlikely to occur, this is discussed more in the next section 1.2.2. To observe homogeneous nucleation, heterogeneous nucleation must be eliminated. The electrostatic levitation is a well-suited technique to study homogeneous nucleation [16]. It is calibrated under ultra-high vacuum to avoid heterogeneous nucleation taking place on the container walls. Secondly, by the mechanism of "self-surface cleaning" at very high temperatures nucleation on the surface can be completely avoided. The process starts with heating the solid sample to its melting temperature, T_m , once the solid has melt, the liquid sample is heated to a temperature much greater than the nucleation temperature, T_l , the liquid is then let to cool completely. During the undercooling i.e. $\Delta T = T_m - T_l$, the nucleated crystal quickly starts to grow because of the very huge thermodynamic driving force at such huge temperature gradient. The rate of homogeneous nucleation is given by:

$$I_{hom} = \frac{4\pi (r^*)^2 N_A v_0}{V_A^{2/3} N_{hom}} \left(\frac{\Delta G^*}{3\pi k_B T}\right)^{1/2} \exp\left[-\left(\frac{\Delta G^* + \Delta G'_m}{k_B T}\right)\right] \approx K \exp\left(\frac{-\Delta G^*}{k_B T}\right) \tag{1.8}$$

where v_0 is the vibrational frequency, N_A is the Avogadro constant, N_{hom} is the number of atoms in critical size nuclei, $\Delta G'_m$ is the free energy of activation of atom jumping over the liquid-nucleus interface, k_B is the Boltzmann constant and K is a constant in the order of 10^{39} $m^{-3}s^{-1}$ to $10^{42} m^{-3}s^{-1}$.

[1]

[1] For the approximation of eq. 1.8, it was assume that $\Delta G'$ is less significant compare to ΔG^*, which is highly temperature dependent and is therefore more dominant. It was also verified by calculation.

1.2.2 Heterogeneous nucleation

Heterogeneous nucleation can be seen as a surface catalyzed process. How much a surface can help nucleation depends on the contact angle of the nucleus on the mold wall. The mold wall could be an insoluble oxide that can become a substrate for heterogeneous nucleation. The smaller this angle, the lower is the free energy change and the nucleation barrier.
Heterogeneous nucleation takes place more often than homogeneous nucleation. It is much faster than homogeneous nucleation because the nucleation barrier is much smaller at the surface. This is due to the fact that the nucleation barrier comes from the surface term which is positive. In homogeneous nucleation, the surface is assumed to be a sphere and hence has area $4\pi r^2$. However, in heterogeneous nucleation the droplets are not a full sphere so the interface is less than $4\pi r^2$. This geometrical factor decreases the interface energy as well as the interfacial free energy that as a result decreases the nucleation barrier. This reduced barrier facilitates nucleation.

For heterogeneous nucleation the release of free energy, ΔG^*_{het}, due to the formation of hemispherical solid can be expressed as:

$$\Delta G^*_{het} = -V_S \Delta G_V + A_{SL}\gamma_{SL} + A_{SM}(\gamma_{SM} - \gamma_{LM})$$

V_S is the volume of the sphere, A_{SL} is the area of the solid-liquid and A_{SM} is the area for the solid-mold interface. There are three different interfacial energies to consider, shown in fig. 1.5, namely γ_{SL}, the surface energy between solid and liquid, γ_{SM}, the surface energy between solid and mold and γ_{LM}, the surface energy for liquid and mold.

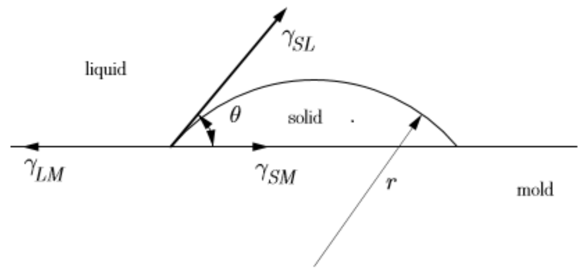

Figure 1.5: *spherical solid cap with radius r and contact angle θ with the mold wall [9]*

The contact angle, θ , can be expressed in terms of the three interface energy [2]:

$$\gamma_{LM} = \gamma_{SM} + \gamma_{SL} \cdot cos\theta \tag{1.9}$$

which can give the following expression for the nucleation barrier:

$$\Delta G^*_{het} = \frac{16\pi\gamma^3_{SL}}{3\Delta G^2_V} S(\theta) = \Delta G^*_{hom} S(\theta) \tag{1.10}$$

which in principle is the product of homogeneous nucleation barrier and the contact angle. The energy barrier is reduced by the factor, $S(\theta)$, which is function dependent on the contact angle and is given by:

$$S(\theta) = \frac{1}{4}(2 + cos(\theta))(1 - cos\theta)^2 \tag{1.11}$$

Fig. 1.6 shows how $S(\theta)$ varies with θ.

[2] eq. 1.9 is known as the Young's equation, for full derivation of eq. 1.10, see ref. [15]. Note here that the critical radius for heterogeneous nucleation remains same as for homogeneous nucleation while the critical volume decreases due to surface wetting.

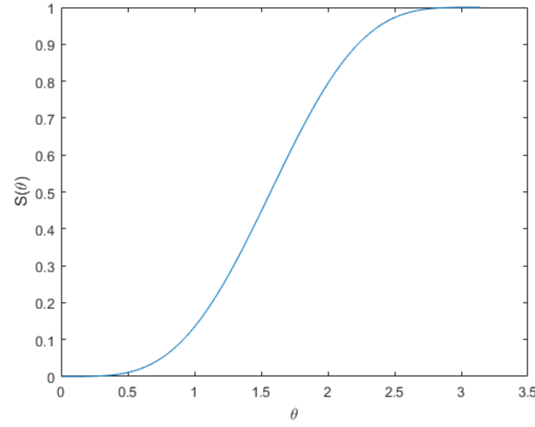

Figure 1.6: *shows the contact angle* (θ) *versus the function of contact angle* $S(\theta)$. $S(\theta)$ *ranges from 0 to 1*

The expression for heterogeneous nucleation is given by:

$$I_{het} = \frac{A^* \upsilon_0}{V_A^{4/3} N_{het}} \Big(\frac{\Delta G^*_{het}}{3\pi k_B T}\Big)^{1/2} exp\Big[-\Big(\frac{\Delta G^*_{het} + \Delta G'_m}{k_B T}\Big)\Big] \tag{1.12}$$

where $N_{het} = NS(\theta)$.
G^*_{het} is much smaller then G^*_{hom} because of the factor $S(\theta)$ that appears in the heterogeneous nucleation barrier. As a result, heterogeneous nucleation is achieved at a smaller undercooling than homogeneous nucleation. In reality, homogeneous nucleation of the solid phase barely takes place in the liquid bulk. Mostly nucleation starts on the walls of the container or on high melting point oxides particles dispersed in the melt. These inhomogeneous sites decrease the nucleation barrier by interfering with the formation of nucleus. Fig. 1.7 below shows free energy for heterogeneous nucleation being lower than the homogeneous nucleation.

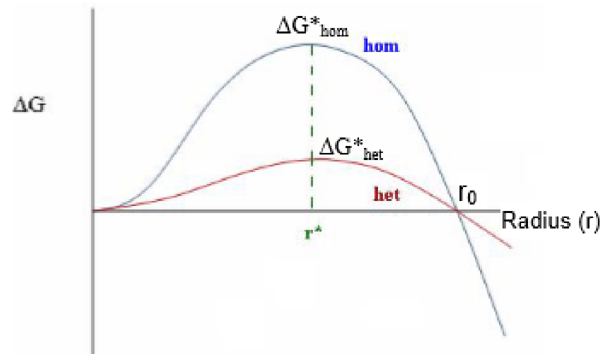

Figure 1.7: *free energy versus radius for homogeneous and heterogeneous nucleation. Contact angle effect the rate of heterogeneous nucleation by reducing the energy barrier [15]*

According to Poisson [17], the probability to find a particle on particular site is $exp\Big(\frac{-\Delta G^*}{kT}\Big)$. Accordingly no matter if the number of possible sites is much smaller for heterogeneous nucleation, its probability is always higher than that for homogeneous and therefore heterogeneous nucleation dominates.

1.3 Growth velocity

After the formation of a nucleus, the phase transition proceeds with the growth process. Epitaxial growth is a process of attaching atoms to previously existed crystal. Close to the solid-liquid interface, atoms from the solid can either attach or dissolve. The rate of attachment depends on the activation energy of jumping across solid-liquid interface, ΔG_M, whereas the dissolving rate in addition, depends on the energy change per atom, Δg_A. The difference between the attaching and dissolving rate determines the epitaxial growth rate. The growth velocity, U , is as following [3]:

$$U = a_o v_o \cdot \exp\left(\frac{-\Delta G_M^{'}}{k_B T}\right)\left[1 - exp\left(\frac{-\Delta G_V V_m}{k_B T}\right)\right] \tag{1.13}$$

where a_0 is the inter atomic distance and $\Delta g_A = (\frac{T - T_m}{\Delta T_m})\Delta h_F$.
As the temperature decreases, the energy barrier for rate of attachment, $\Delta G_M'$, is approximately unchanged whereas the energy barrier for the rate of dissolving $\Delta G_M' + \Delta g_A$ is increased, this gives the driving force for the epitaxial growth. For the growth to take place, this driving force needs to be sufficient to dissolve an atom and still create the new attachment site. Fig. 1.8 below shows the attachment and detachment of atoms in crystal along with nucleation process that occurs.

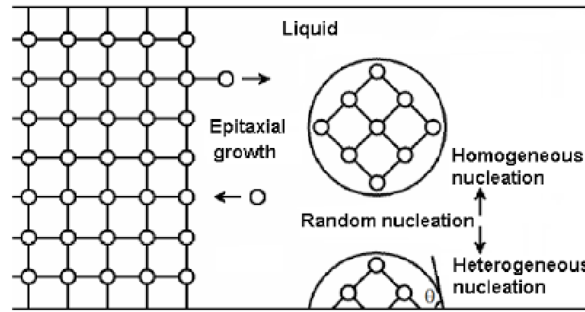

Figure 1.8: *The process of solidification by epitaxial growth and nucleation [18]*

In the above figure, schematics for growth and nucleation process is illustrated. In principle, heterogeneous nucleation is also an attachment process just like the growth rate apart from the fact that it does not have a preexisting crystal template. The homogeneous nucleation is more like an "assembling" process that results in nuclei formation.

[3] In the above eq. 1.13 according to ref. [9] for simplification we have assumed that the kinetic barrier for atom jump across solid-liquid surface is equal to the free energy of activation for jumping of atoms. In practice they may have different values.

Chapter 2

Method

This chapter discusses Rapid Melt Growth and the parameters required for the thermodynamic calculations. The rapid melt growth technique is discussed first followed by the motivation for the choice of the parameters.

2.1 Rapid melt growth

Rapid melt growth was first used by Lie et al in 2004 for III–V crystal growth [19]. It is a simple and robust technique that gives good possibilities for heterogeneous integration. The process for RMG is shown step wise in fig. 2.1 below. In this technique, firstly an amorphous dielectric layer e.g. SiO_2 that acts as an isolation layer is deposited on top of the substrate e.g. Si. RMG seed windows are selectively opened via etching the dielectric layer, this expose the underlying Si layer for lateral epitaxial growth of InSb. Polycrystalline InSb is usually deposited by Molecular Beam Epitaxy or Sputtering under equilibrium condition and uniformly deposited and patterned on top of the amorphous layer. InSb is etched followed by the deposition of SiO_2. At last a heating source e.g. Rapid Thermal Annealing or RTA is used to heat the entire structure about the melting temperature of InSb. The model is let to solidify, during the solidification process crystal growth of InSb appears from initially seeded region that starts to propagate along the length of the crystal.

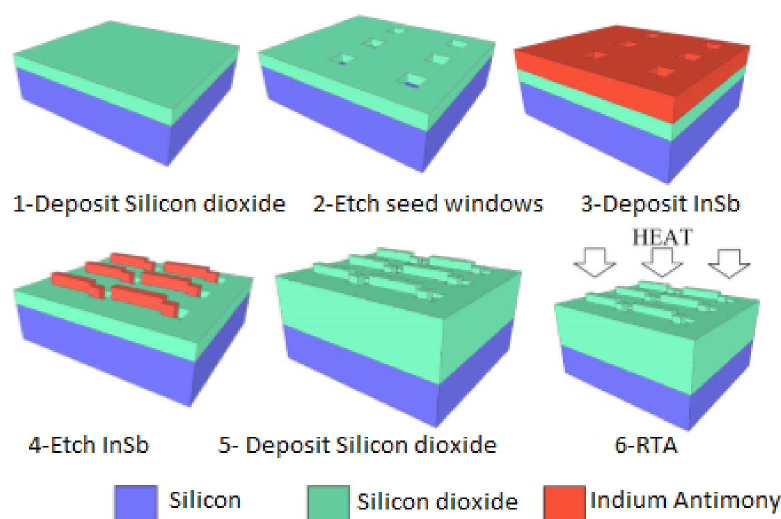

Figure 2.1: *illustrates the summary of rapid melt growth process for InSb [20]*

Rapid melt growth has several important features that ensures the development of high quality single-crystal growth on the target material. Firstly, the seeded region gives a crystallization template to controls orientation see fig. 2.2 below. Second, a melted material treated under equilibrium condition with minor undercooling and temperature gradient at the growth interface helps obtain high quality growth during epitaxy. Third, self-aligned micro crucible holds the melt and finds the crystal growth direction. Finally, necking close to the seeding region helps avoid defects. Defect necking makes sure that lattice mismatch that could possibly give rise to dislocation between the seed and the material does not travel further into the melt [21]. To obtain a high quality single crystal form RMG, the growth velocity must be high enough to avoid random nucleation taking place ahead of epitaxial growth front the epitaxial.

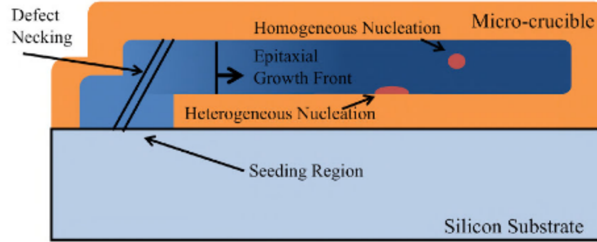

Figure 2.2: *Shows the defect necking being done close to the seed region. The Homogeneous nucleation on bulk of the melt, the heterogeneous nucleation on the surface of the melt. Both nucleation is ahead of the epitaxial growth front. RMG is primarily a competition between the epitaxial growth initiating from seed region and heterogeneous nucleation ahead of the growth front [22]*

Benefits over other techniques

Rapid melt growth has benefits over other epitaxial techniques. Most epitaxial growth techniques require a certain temperature scale for the growth and then require annealing to remove defects. Whereas in RMG process the annealing step is taken over by one sharp temperature peak to give direct phase transformation. Secondly, in RMG only small fraction of the target material is exposed to silicon. This gives rise to more uniform growth with no voids at the boundary.

2.2 Parameter Analysis

The thermodynamic parameters for epitaxial growth and nucleation are not easily available in literature and are mostly found by experiment. In this thesis, the parameters are found based on relevant equations and appropriate assumptions from the literatures.

In the growth velocity, eq. 1.13, many unknown parameters exist. To produce growth velocity graph, the parameters as the lattice constant, a_0 , the Boltzmann constant, k_B , vibration frequency, v_0 , the kinetic barrier for jumping of atoms, $\Delta G'_m$, and the enthalpy of fusion, Δh_f , needs to be known. It is important that the parameters are correct or are close to the expected values.

Parameters as a_0 and k_B are standard and are set to 6.479×10^{-10} m and $1.3805423 \times 10^{-23}$ J/K respectively. The radius from eq. 1.6 is found to be 80 nm, the melting temperature, T_m , is found to be 805 K [23]. The rest of the parameters such as vibration frequency, v_0 , the kinetic barrier for jumping of atoms, $\Delta G'_m$, and the enthalpy of fusion, Δh_f , are not trivial to find. It is critical that these parameters are correct or at least reasonable.

$\Delta G'_m$ was found to be 1.76×10^{-20}J/atom [24], this value is taken even though it corresponds to the melting temperature of 753 K. υ_0 is approximated to 1×10^{12} Hz, a typical vibrational frequency of atoms. Δh_f was precisely found to be 4.23×10^{-20} J/atom [25]. For the calculation of the free energy change per atom, Δg_A , the relation, $\Delta g_A \approx (\Delta T/T_m)\Delta h_F$ [9], is used, where the undercooling is given by $\Delta T = T_m - T_l$. Substituting these along with Δh_F gives values for Δg_A. All these parameters are compiled in MATLAB to produce a graph of growth velocity in m/s versus temperature in K.

The parameters as the solid-liquid surface energy, γ_{SL} , the atomic volume, V_A , and the contact angle, θ , are vital for the calculation of homogeneous and heterogeneous nucleation rate. The solid-liquid interface energy was estimated by $\gamma_{SL} = F_b\Delta h_f\sigma = F_b\Delta h_f\frac{1}{V_A^{2/3}}$ [10], where F_b is the fraction of bonds broken at the interface and σ is the atomic surface density. Here a good approximation for F_b is given as ≈ 0.5 [10]. Substituting the known values into the expression for γ_{SL} gives the interface energy as 0.127 J/m^2. The atomic volume V_A is the inverse of the density in thermodynamics. It is given by $V_A = 1/\rho = a_0/4 = 6.7993\times10^{-29}$ cm^3/atom. The contact angle is however difficult to find. This parameter is very critical for heterogeneous nucleation which is the dominant nucleation and therefore it should have a reasonable value. In this thesis, it is found to be 347°. The following section will propose alternate ways to calculate the contact angle and the way that it is implemented in this thesis.

Hysteresis in contact angle

The contact angle is a complex phenomenon. Earlier θ was expressed by Young's eq. 1.9. However, Young's equations is valid for static particles therefore it only determines a single and unique contact angle. In reality, the liquid moves so the three-phase contact angle is in actual motion therefore the contact angle is instead dynamic. The contact angle has been investigated carefully, and that reason to the contact angle hysteresis is the surface roughness or heterogeneity. These roughness's gives barrier in motion. In such cases Young's equation can be deceptive as it does not take surface topography into account [26].

Apart from Young's equation, the following equation has been tested to produce good result for the contact angle [27].

$$cos(\theta) = a\frac{r^*}{R} + b \tag{2.1}$$

This is a linear equation. The parameters a and b in eq. 2.1 are constants corresponding to the gradient and intercept respectively in the $cos(\theta)$ versus $\frac{r*}{R}$. This equation can be used to find the contact angle for any seed particle with radius R. However the accuracy of this equation is highly sensitive to the accuracy and precision of the parameters a and b [27].

Nevertheless, for this thesis, this equation is not the solution to the problem, and in fact adds complexity to the calculation for the contact angle since we are only working with the critical radius r^*, and not r^*/R. For simplification, we first assume an ideal solid surface with no surface heterogeneity such that the Young's equation for the contact angle holds. But the problem still remains as all the three surface energies cannot be estimated. Surface energies are measured indirectly from the contact angle and the contact angle in that case is measured with advanced imaging techniques, as interference microscopy and in this thesis no experimental set up was

used.

To avoid all these problems, first order approximation for angle is made based on lattice mismatch between Si/ Ge and Si/InSb. Lattice mismatch, M, can be defined as:

$M = \frac{a_{film} - a_{substrate}}{a_{substrate}} \times 100,$

$M_{Ge} = \frac{5.65 - 5.43}{5.43} \times 100 \approx 4\%,$

$M_{InSb} = \frac{6.48 - 5.43}{5.43} \times 100 \approx 19\%.$

For $M_{Ge} = 4\%$ the angle is $\theta_{Ge} = 72°$ [9] and therefore for $M_{InSb} = 19\%$ the angle is found to be $\theta_{InSb} = 347°$.

Chapter 3

Results and Discussion

The results for nucleation and growth as a function of temperature is presented below. In the analysis section, relevant expressions are described to understand the effect of the cooling rate on maximum crystal length. Finally, the obtained results are discussed.

3.1 Results

The table below summarizes the calculated parameters for nucleation and growth velocity.

Table 3.1: *summary of the required parameters for RMG of InSb*

Parameters	Values	Unit	Ref
υ_0	1×10^{12}	Hz	[24] [25]
$\Delta G'_m$	1.76×10^{-20}	$J/atom$	[26]
Δh_F	4.23×10^{-20}	$J/atom$	[27]
T_m	805	K	[23]
θ	347	degrees (°)	-
γ_{SL}	0.127	J/m^2	[10]
V_A	4.5168×10^{-29}	$cm^3/atom$	[5]

For the growth velocity, U , eq. 1.13 was used to along with the required parameters from table 3.1 to produce the blue curve below. For homogeneous and heterogeneous nucleation, eq. 1.8 and eq. 1.12 were used along with the required parameters from table 3.1 to plot the black and green graph respectively.

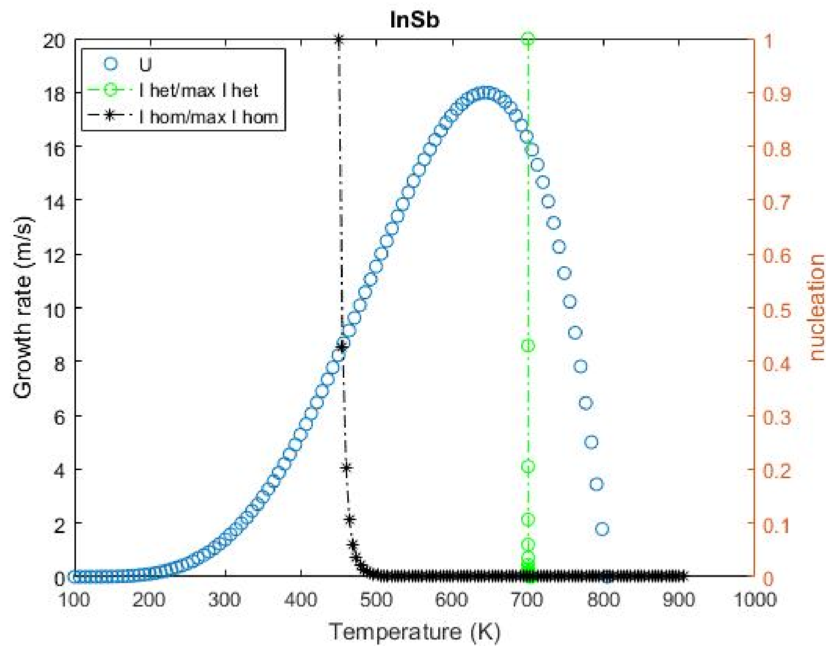

Figure 3.1: *Shows the growth velocity, homogeneous nucleation rate and heterogeneous nucleation rate as function of temperature for InSb*

Firstly from the growth velocity graph, we can see that the plot ends at the melting temperature. The figure clearly shows a process window with very fast growth velocity when the undercooling is about 200 K to 250 K below the melting temperature. The growth peaks at 645 K and the corresponding growth velocity is 16.7 m/s. At elevated temperature, the growth velocity is very fast featured by the steep gradient. At lower temperature, the growth velocity decreases because the parameters $k_B T$ in eq. 1.13 becomes powerful.

Secondly, from the nucleation rates graph, it is evident that within a short temperature window the rise in the nucleation rate is drastic. This is because the nucleation barrier, G^* , and the critical radius, r^* , are highly sensitive to temperature. Before going to further details, these features are first shown in fig. 3.2 and fig. 3.3 below.

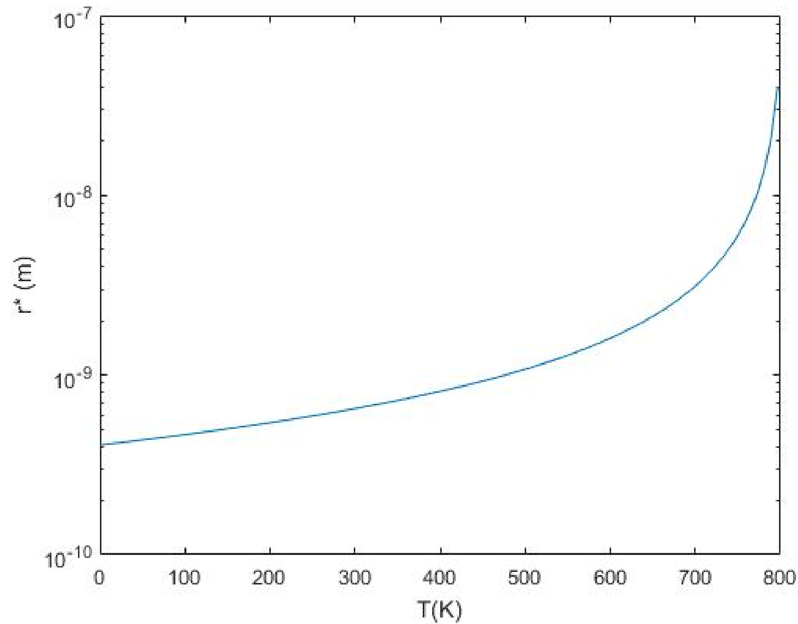

Figure 3.2: *The graph shows radius as a function of temperature. Within small change in critical radius there is a huge temperature change. The change corresponds to approximately* 10^{-7} *m to* 10^{-9} *m over a huge temperature range of 400 K to 800 K. This implies radius is highly sensitive to temperature after 400 K*

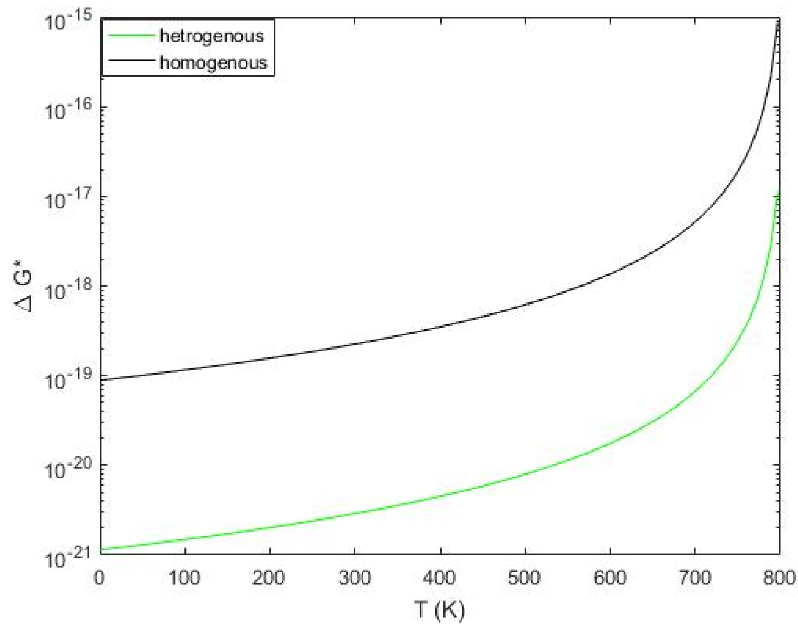

Figure 3.3: *The graph shows the nucleation barrier for homogeneous and heterogeneous as a function of temperature. Firstly, we notice the large temperature sensitivity of the nucleation barrier after 500 K. Secondly, we observe that heterogeneous nucleation barrier is lower than the homogeneous nucleation barrier in accordance with the theory. The barrier is reduced by factor of* $S(\theta)$ *which is calculated to be 0.0027*

Lastly, it is observed that heterogeneous nucleation is more likely to occur than homogeneous since the energy barrier is reduced. As a result, heterogeneous nucleation is observed at much smaller undercooing. From fig. 3.1, the undercooling is around 108 K for heterogeneous and around 312 K for homogeneous nucleation. It is this temperature window of 108 K where growth is maximum and nucleation is negligible.

Nonetheless, this temperature window does not help us understand grow long single crystal strips which is important contribution of RMG. This is due to the fact that the ultimate length of the crystal depends not only on growth velocity but also on the growth time and this information does not exist in the temperature window. But this can be achieved, in the further analysis section, it is described that certain adjustments can be made to calculate maximum cooling rate that can give the longest length of the single crystal before a homogeneous nucleation takes place.

3.2 Further analysis

Previously we showed that classical nucleation theory gives a process window where growth velocity is dominant over small nucleation rates. However, this gives us a limited information and does not provide further detail of how long can a crystal travel given certain cooling rate and dimension. To expand the results from RMG, we could calculate the maximum length of a single crystal before the growth velocity is interrupted by random nucleation. To achieve this in a more quantifiable manner, other parameters beside temperature such as time and geometry should be included. Under the assumption that all sources of heat is stopped after melting, there exists a certain time that corresponds to a specific temperature. This implies that time and temperature are replaceable. The following equation gives a relation between change in time δt and temperature δt as a function of cooling rate CR.

$$CR \approx \frac{\delta T}{\delta t} \tag{3.1}$$

According to this equation, if for example a cooling of 50 K is done at a cooling rate of 10 K/s than at 100 K/s , then the cooling time is larger by factor of 10 for 10 K/s. From this it is deduced that within same temperature interval, it is the difference in time that determines the final length of the crystal. To find the final epitaxial length of the crystal, the growth velocity in eq. 1.13 can be integrated with respect to this time. The expression for the length, L , of the crystal could be derived to give:

$$\delta L = U \cdot \delta t = U \frac{1}{CR} \delta T \tag{3.2}$$

The growth velocity, U , which was a function of temperature is now a function of time. The equation shows that the length of crystal is highly dependent on the cooling rate. Worth noting that δT does not contribute to the change in crystal length, it is because even though δT increases the total number of steps for summation, it at the same time reduces the value of each individual L-step. To be more precise, the increase in cooling rate decreases the length of the crystal to few micrometers. Second, temperature does not affect the final length of the crystal. This holds because crystal growth necessitates both growth velocity and time.

To model this assuming nucleation rates and growth rate from thermodynamic calculation, MATLAB code was restructured such that growth and nucleation rates takes temperature, T, as a first parameter. Growth is assumed to start when number of heterogeneous nuclei is greater or equal to 1 and finish when number of homogeneous nuclei is greater or equal to 1. This gives a maximum limit on the possible length, L , of the crystal, the growth time, t, and the end temperature, T. Because the cooling rate is dependent on factors as structure and thermal excitation,

the cooling rate in eq. 3.2 to see its effect on propagation of single crystal. The figure below represents the effect of cooling rate on maximum single crystal length.

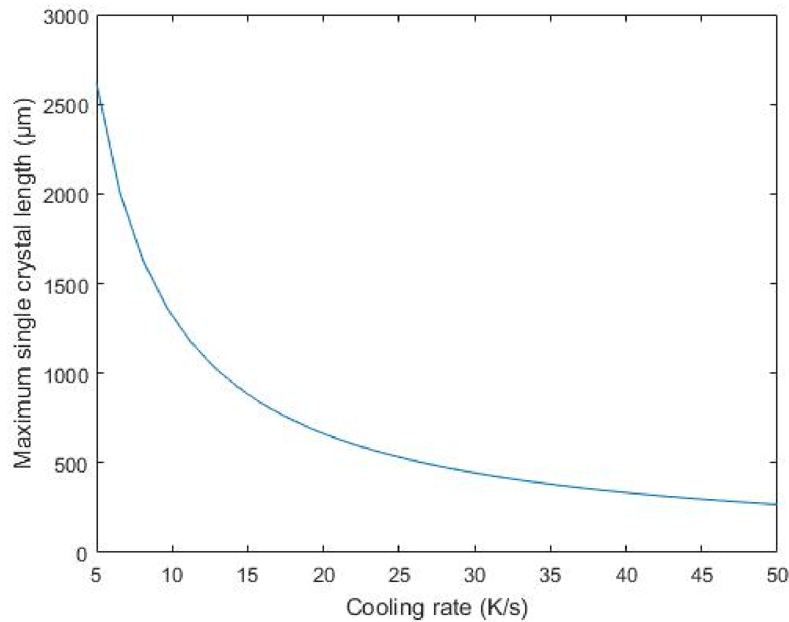

Figure 3.4: *Shows the maximum single crystal length of InSb as a function of cooling rate in the range from 5 to 50*

This graph illustrates an important characteristics of rapid melt growth. For the same temperature window lower cooling rate results in larger crystal length. From the graph at cooling rate of 5 K/s the maximum length is 2.61 mm while for cooling rate of 50 K/s, the maximum length is 0.25 mm. This confirms the relation 3.2. Apart from this at higher cooling rate, the time get so small that even with higher growth velocity, epitaxial growth cannot be attained.
The following values were calculated for the above graph:
The final crystal length L = 2.61 mm
The total growth time $t = 6$ s
The final temperature at which homogeneous nucleation is certain $T = 486$ K
So the final length of InSb before homogeneous nucleation takes place at temperature of T = 486 K is found to be 2.61 mm. The corresponding growth time is t = 6 s.

3.3 Discussion

Considering growth velocity and nucleation rate first, in fig. 3.1, the calculated growth velocity is in the range for undercooled InSb liquid. The peak value for InSb in ref. [28] was obtained to be 653 K whereas we obtained it to be 645 K. The temperature window obtained was 108 K, according to ref. [29], undercooling before nucleation takes place are generally small and a temperature window of less than 300 K is a good estimate. So we can deduce that the temperature window of 108 K is reasonable and that in this window the growth rate of InSb is maximum and nucleation is minimum. The undercooling obtained for homogeneous was large than heterogeneous, in accordance to the theory. However, in the theory, the pre factor K for homogeneous nucleation is of the order 10^{39} $m^{-3}s^{-1}$ to $10^{42}m^{-3}s^{-1}$ where as we obtained it to be 10^{36} $m^{-3}s^{-1}$. For heterogeneous the pre factor should be much less than the one for homogeneous and we obtained it to be 10^{26} $m^{-3}s^{-1}$, which is well lower.

Next coming to the results for the maximum length of the crystal, the length was found to be 2.61 mm. Generally depending upon the application of InSb the length can vary but at least 10 μm to 100 μm is necessary.
The length of 2.61 mm obtained is a long enough distance to give sufficient dimension for many devise fabrications. The final length was highly sensitive to parameters as the vibrational frequency and the free energy of jumping of atoms. Fig. 3.5 shows the effect of increasing both parameters.

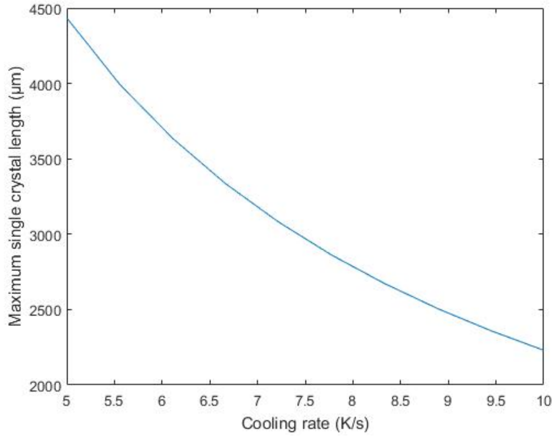

***(a)** L versus CR for* $\Delta G' m = 3 \times 10^{-20} J/at$

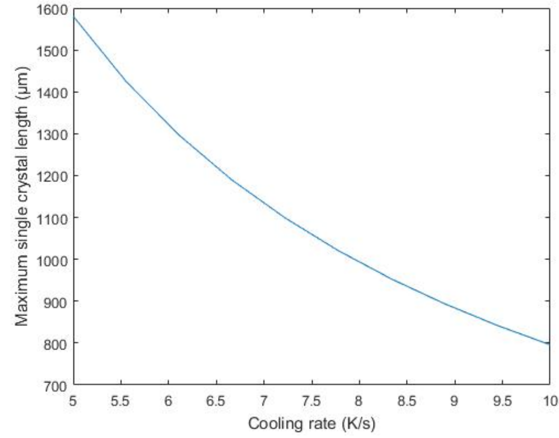

***(b)** L versus CR for* $v_0 = 1.7 \times 10^{12} Hz$

***Figure 3.5:** Figure a) shows the result of increasing* $\Delta G' m$*= from* $1.76 \times 10^{-20} J/at$ *to* $3 \times 10^{-20} J/at$ *. Figure b) shows the result of increasing* v_0 *from* 1×10^{12} *Hz to* 1.7×10^{12} *Hz*

From figure a, we can see that at the same cooling rate of 5 K/s, slightly increasing the free energy of activation substantially increases the length of the crystal from 2.61 mm to 4.41 mm. This gives a longer crystal. Some application requires longer crystals, this parameter could be re checked also because it was found for a different melting temperature. From figure b, increasing the vibrational frequency from 1×10^{12} Hz to 1.7×10^{12} Hz, decreases the length to 1.58 mm, the exact value should therefore be looked for since the length of the crystal is sensitive to this parameter.

Chapter 4

Conclusion and Outlook

The results by rapid melt growth confirmed the presence of a temperature window. The epitaxial growth traveled for a distance of 2.61 mm before it was interrupted by random nucleation. This length depending on the application is long enough to allow quality devise integration. Although some parameters are questioned for their reliability, the important thermodynamic parameters have been analyzed to help us design some experiment. Rapid melt growth of InSb can be applied to other potential channel material that have similar temperature dependency of growth velocity and nucleation. However, experiments along with more research can help us improve the results. Since the contact angle was hard to find, one way to find the contact angle with accuracy of ±2° [27] via experiment is shown below:

Measurement with Telescope-Goniometer

Figure 4.1: *Telescope-Goniometer [27]*

Telescope-Goniometer in fig. 4.1 is a simple and convenient technique to measure the three phases of the contact angle. The equipment comprises of a horizontal stage to place the sample, a micrometer pipette, a light source and a telescope with eye piece protractor. After the alignment of the setup, the contact angle is simply measured by reading the protractor via the eyepiece [27].

Bibliography

[1] X. Bai and J. D. Plummer, "Rapid melt growth of single crystal InGaAs on Si substrates," *Nano lett*, feb (2009).

[2] H. Joyce, Q. Gao, and J. Zou, "Unexpected benefits of rapid growth rate for III-V nanowires," *Hindawi publishing corporation*, 6 sep (2016).

[3] S. Mokkapati and C. Jagadish, "III-V compound SC for optoelectronic devices," *Materials Today*, vol. 12, no. 4, pp. 22 – 32, june (2009).

[4] G. Sareminia1, F. Zahedi1, S. Eminov, and A. Karamian, "Cleaning method of InSb $[\bar{1}\bar{1}\bar{1}]$ of n-InSb [111] A/B for the growth of epitaxial layers by liquid phase epitaxy," *Journal of Semiconductors*, vol. 32, no. 5, may (2011).

[5] "Indium antimonide InSb semiconductors," *Azo materials*, vol. 32, no. 5, 12 april (2013).

[6] Adachi and Sadao, "Indium antimonide InSb optical constants of crystalline and amorphous semiconductors: Numerical data and graphical information," *Springer US*, pp. 268–278, (1999). `http://dx.doi.org/10.1007/978-1-4615-5247-5_27`, version 1.6.0.

[7] H. Nilsson, P. Caroff, C. Thelander, E. Lind, O. Karlström, and L. Wernersson, "Temperature dependent properties of InSb and InAs nanowire field-effect transistors," *Applied Physics Letter*, vol. 96, no. 15, (2010).

[8] M. Shafa, S. Akbar, L. Gao, M. Alam, and Z. Wang, "Indium antimonide nanowires: Synthesis and properties," *Nanoscale Res Lett*, 24 mar (2016).

[9] L. Yaocheng, D. Michael, and J. D. Plummer, "Rapid melt growth of germanium crystals with self-aligned micro crucibles on Si substrates," *Journal of the Electrochemical society*, vol. 152, 12 jan (2015).

[10] "Chapter 6 solidification," *Jrgreer Caltech Edu*. `http://www.jrgreer.caltech.edu/content/teaching/MS133Files/Notes/Lect9MS133JRG.pdf`.

[11] D. Richard and P. Sear, "Classical nucleation theory," 6 oct (2000).

[12] Y.Liu, "Silicon and germanium crystalization technique for advanced device application," *Dept of mat Sci and Eng, Stanford Univ*, (2005).

[13] J.Feng, "High performance germanium on insulator MOSFETS for three dimensional integrated circuit based on rapid melt growth," *Dept of Elec Eng, Stanford Univ*, (2009).

[14] M. Krbal, A. Kolobov, B. Hyot, B. André, P. Fons, R. E. Simpson, T. Uruga, H. Tanida, and J. Tominaga, "Amorphous insb: Longer bonds yet higher density," *Journal of applied physics*, vol. 108, (2010).

[15] "Lecture 12: Heterogeneous nucleation: a surface catalyzed process," `http://www.eng.utah.edu/~lzang/images/lecture-12.pdf`.

[16] D. Herlach, "Containerless undercooling of drops and droplets,"

[17] V. Dubrovskii, "Nucleation theory and growth of nanostructures," *NanoScience and Technology, Springer-Verlag Berlin Heidelberg*, (2014).

[18] S. Chen, "Design and process for three dimensional heterogeneous integration," *Department of the Elec Eng at Stanford University society*, aug (2010).

[19] L. Yaocheng, D. Michael, and J. D. Plummer, "High quality single crystal ge on insulator by liquid-phase epitaxy on Si substrate," *Applied Physics letter*, April (2004).

[20] G. Callum, L. johns, and M. Nedeljkovic, "Next generation device grade silicon-germanium on insulator," *Scientific Reports*, 6 Feb (2015).

[21] M.Predeleanu, "Advanced methods in materials processing defects," *studies in Applied Mechanics*, mar (2000).

[22] H. Yin and S. Koh, "Rapid melt growth of silicon germanium for heterogeneous integration on silicon," *Department of the Elec Eng at Stanford University society*, aug (2011).

[23] M. Ghasemi, Z. Zanolli, M. Stankovski, and J. Johansson, "Size- and shape-dependent phase diagram of In–Sb nano-alloys," *Royal Society of Chemistry*, vol. 7, (2015).

[24] G. Sapkota and U. Philipose, "Synthesis of metallic, semiconducting, and semi-metallic nanowires through control of InSb growth parameters," *Semiconductor Science and Technology*, vol. 29, no. 3, p. 035001, (2014).

[25] "Indium antimonide, InSb - matweb,"

[26] Y. Yuan and T. Lee, "Contact angle and wetting properties," *Springer Series in Surface Sciences*, (2013).

[27] A. Hienola, E. Wagner, and M. Kulmala, "Estimation of line tension and contact angle from heterogeneous nucleation experimental data," *The journal of chemical physics 094705*, vol. 126, (2007).

[28] A. Vogel, J. Boor, and V. Schmidt, "Ag-assisted cbe growth of ordered insb nanowire arrays," *Nanotechnology*, Jan (2011).

[29] J. Graves and M. Madison, ""undercooling and solidification behavior in the InSb-Sb system"," *NASA Contractor Report 175013*, Sep (1985).